BIOCHEMISTRY

Article

Functional Effects of Periodic Tryptophan Substitutions in the M4 Transmembrane Domain of the *Torpedo californica* Nicotinic Acetylcholine Receptor

Shiori Tamamizu, Gisila R. Guzmn, John Santiago, Legier V. Rojas, Mark G. McNamee, and Jos A. Lasalde-Dominicci

More About This Article

Additional resources and features associated with this article are available within the HTML version:

- Supporting Information
- Links to the 6 articles that cite this article, as of the time of this article download
- Access to high resolution figures
- Links to articles and content related to this article
- Copyright permission to reproduce figures and/or text from this article

View the Full Text HTML

ACS Publications
High quality. High impact.

Functional Effects of Periodic Tryptophan Substitutions in the α M4 Transmembrane Domain of the *Torpedo californica* Nicotinic Acetylcholine Receptor[†]

Shiori Tamamizu,[‡,§] Gisila R. Guzmán,[‖] John Santiago,[‖] Legier V. Rojas,[⊥] Mark G. McNamee,[‡] and José A. Lasalde-Dominicci*[,‖]

Section of Molecular and Cellular Biology, University of California, Davis, California 95616, Department of Biology, University of Puerto Rico, P.O. Box 23360, San Juan, Puerto Rico 00931-3360, and Department of Physiology, School of Medicine, Universidad Central del Caribe, Bayamón, Puerto Rico 00960-6032

ABSTRACT: Previous amino acid substitutions at the M4 domain of the *Torpedo californica* and mouse acetylcholine receptor suggested that the location of the substitution relative to the membrane−lipid interface and perhaps to the ion pore can be critical to the channel gating mechanism [Lasalde, J. A., Tamamizu, S., Butler, D. H., Vibat, C. R. T., Hung, B., and McNamee, M. G. (1996) *Biochemistry 35*, 14139−14148; Ortiz-Miranda, S. I., Lasalde, J. A., Pappone, P. A., and McNamee, M. G. (1997) *J. Membr. Biol. 158*, 17−30; Tamamizu, S., Lee, Y. H., Hung, B., McNamee, M. G., and Lasalde-Dominicci, J. A. (1999) *J. Membr. Biol. 170*, 157−164]. In this study, we introduce tryptophan substitutions at 12 positions (C412W, M415W, L416W, I417W, C418W, I419W, I420W, G421W, T422W, V423W, S424W, and V425W) along this postulated lipid-exposed segment M4 so that we can examine functional consequences on channel gating. The expression levels of mutants C412W, G421W, S424W, and V425W were almost the same as that of the wild type, whereas other mutants (M415W, L416W, C418W, I419W, I420W, T422W, and V423W) had relatively lower expression levels compared to that of the wild type as measured by iodinated α-bungarotoxin binding ([125I]-α-BgTx). Two positions (L416W and I419W) had less than 20% of the wild type expression level. I417W gave no detectable [125I]BgTx binding on the surface of oocyte, suggesting that this position might be involved in the AChR assembly, oligomerization, or transport to the cell membrane. The αV425W mutant exhibited a significant increase in the open channel probability with a moderate increase in the macroscopic response at higher ACh concentrations very likely due to channel block. The periodicity for the alteration of receptor assembly and ion channel function seems to favor a potential α-helical structure. Mutants that have lower levels of expression are clustered on one side of the postulated α-helical structure. Mutations that display normal expression and functional activity have been shown previously to face the membrane lipids by independent labeling studies. The functional analysis of these mutations will be presented and discussed in terms of possible structural models.

The nicotinic acetylcholine receptor (nAChR) from muscle and electric ray organ is an integral membrane protein comprised of four homologous polypeptide subunits with an $\alpha_2\beta\gamma\delta$ stoichiometry (for reviews, see refs *1−6*). A consensus model for the nAChR topology obtained from hydrophobicity profiles for protein sequences deduced from cDNA sequences indicates that each subunit contains at least four membrane-spanning regions (MSRs) denoted M1−M4 with both N- and C-termini located on the extracellular side (*7*).

Among the four postulated transmembrane domains of the *Torpedo californica* nAChR, M4 is the most hydrophobic and has the lowest level of side chain conservation. Photoaffinity labeling experiments have shown that M4 has the largest contact with lipids (*8*) and the pattern of 3-(trifluoromethyl)-3-*m*-[125I]iodophenyldiazirine ([125I]TID) labeling on the M4 domain is compatible with an α-helical structure (*9*). We have shown that a single amino acid substitutions at the postulated protein−lipid surface of the nAChR could produce dramatic reduction in the rate of the closing transition of the nAChR channel (*10−12*). These results raised some questions regarding a possible role of the lipid-exposed domains in the gating mechanism. Numerous studies of lipid effects on the nAChR structure and function have demonstrated that membrane lipid composition can modulate receptor function (*5, 13−17*).

A series of amino acids substitutions at the *Torpedo* M4 αG421 position showed that only tryptophan substitution was able to produce a substantial increase (10-fold) in open

channel probability (*18*). A phenylalanine substitution at positions αC418 and αG421 produced a small increase (2-fold) in the open time constant as compared to that with a tryptophan substitution. Polar side chains such as serine and tyrosine at these positions did not produce any significant increase in the open channel constant. These results suggested that polar side chains could not establish appropriate interactions, which leads to the hypothesis that hydrophobicity of the side chain is essential for establishing the interactions that produce a more stable open channel conformation.

The stabilization of the open channel state estimated from the transition state energy for the αC418W mutation is about -0.8 kcal/mol per tryptophan substitution (*18*). Also, this effect was shown to be additive when multiple tryptophan substitutions were combined at equivalent positions of the α and β M4 transmembrane segment, as in the αC418W/βC447W mutation. These data suggest that van der Waals and perhaps dipole interactions at the periphery of the nAChR with the lipid interface could play a significant role in the overall mechanism of the nAChR channel gating. The combined results of the M4 tryptophan substitutions raised the following question: are the effects related to disruption helix–helix contacts, subunits contact, allosteric interactions, or a unique interaction of the tryptophan side chain at the lipid interface of the receptor?

One hypothesis is that the relative position of the tryptophan substitution relative to the ion pore and possibly to the bilayer might be a critical factor in determining the degree of perturbation. Our immediate goal of defining a mechanism by which bulky aromatic replacements in the M4 transmembrane segment produce such effects on the AChR channel gating is to identify the positions in this domain that are capable of modulating ion channel gating.

In the study presented here, we analyzed the periodicity of functional changes at positions αC412–αV425, which covers most of the putative M4 transmembrane domain. Tryptophan replacements on the side of M4 that have been demonstrated to face the lipid environment display a different pattern of modulating channel function compared to that of substitutions that interact with other domains inside the protein. The interpretation of these results provides a better understanding of how tryptophan substitutions in the M4 transmembrane of the nAChR affect the channel gating mechanism. In addition, this study examined functional aspects of what we propose are *hydrophobic allosteric sites* and also additional structural aspects of the M4 that are crucial for AChR assembly and organization.

MATERIALS AND METHODS

Mutations on the Subunit of Torpedo nAChR. Site-directed mutagenesis of the α subunit of *T. californica* nAChR was carried out by mismatch amplification using two sequential PCRs (*19*). The coding region of the α subunit of *Torpedo* nAChR was subcloned from Pα (*20*) into the *Hin*dIII and *Eco*RI sites of the pGEM3Z(−) vector from Promega (Madison, WI). Mutagenic primers containing the desired codon replacement [TGG (Trp) instead of the wild type codon] were extended 11–13 bases on each side of the mismatched region and synthesized by Gibco BRL. Flanking primers were designed to recognize sequences outside the

Table 1: Functional Consequences of M4 Trp Mutants[a]

AChR type	expression level (fmol)	EC$_{50}$ (μM)	Hill coefficient	normalized response (−nA/fmol)[b]
wild type	3.17 ± 0.34	20.6 ± 0.5	1.4 ± 0.2	774 ± 121
C412W	3.60 ± 0.49	13.5 ± 1.1	1.5 ± 0.1	313 ± 55
M415W	1.20 ± 0.13	47.9 ± 5.5	1.7 ± 0.3	1712 ± 243
L416W	0.36 ± 0.08	93.6 ± 9.3	1.4 ± 0.1	2203 ± 281
I417W	NE	ND	ND	ND
C418W	1.14 ± 0.12	3.0 ± 0.9	1.3 ± 0.1	979 ± 84
I419W	0.62 ± 0.08	54.7 ± 7.5	1.2 ± 0.1	1932 ± 261
I420W	0.66 ± 0.15	68.5 ± 13.9	1.3 ± 0.1	832 ± 234
G421W	3.90 ± 0.78	4.8 ± 1.9	1.5 ± 0.05	295 ± 50
T422W	1.37 ± 0.15	51.6 ± 5.1	1.5 ± 0.1	720 ± 97
V423W	0.93 ± 0.16	42.2 ± 3.9	1.3 ± 0.1	809 ± 191
S424W	2.48 ± 0.25	25.3 ± 7.1	1.4 ± 0.1	301 ± 47
V425W	2.97 ± 0.28	14.3 ± 0.5	1.0 ± 0.02	929 ± 308

[a] Values are given as the mean ± the standard error. Femtomoles, for EC$_{50}$ average. The Hill coefficient and normalized response were calculated using 6–35 oocytes. NE, no expression. ND, no detectable current. [b] Normalized peak channel activity for each oocyte was obtained from the ACh-induced current at 300 μM divided by the number of femtomoles of the same oocyte.

*Bgl*II restriction site in the coding region of the α subunit and the *Eco*RI site on the vector portion of the plasmid. Each PCR mix contained 100 μL of 50 mM KCl, 10 mM Tris-HCl (pH 8.3), 1.5 mM MgCl$_2$, 0.01% gelatin, deoxynucleotides (each at 200 nM), 100 ng of DNA template (Pα for single mutations and C418W for double mutations), primers (each at 1.0 μM), and 2.0 units of Pfu DNA polymerase (New England Biolabs, Beverly, MA). Amplification reactions were performed in a DNA thermal cycler (Perkin-Elmer-Cetus) programmed for 30 cycles of a three-step protocol: 1 min at 94 °C, 2 min at 48 °C, and 3 min at 72 °C. The desired PCR products were purified form excised gel slices with Gene-Clean (Bio 101, La Jolla, CA). These DNA fragments were used in a second fusion PCR. The 1.3 kb fusion product was purified from the gel with Gene-Clean and digested with *Bgl*II and *Eco*RI. After digestion, the 0.9 kb mutagenized fragment was inserted into the α subunit gene using T4 DNA ligase (Boehringer Mannheim Biochemicals, Indianapolis, IN). The inserts were sequenced with Sequenase 2.0 (United States Biochemical Corp., Cleveland, OH) to confirm the desired point mutation with no additional mutations.

Expression in Xenopus laevis Oocytes. RNA transcripts were synthesized in vitro as described in ref *10*. The RNA transcripts (10 ng/oocyte at a concentration of 0.2 μg/μL) of α, β, γ, and δ subunits at a 2:1:1:1 ratio were injected into *Xenopus* oocytes. The concentrations of RNA mixes were increased to 0.8 μg/μL to give 40 ng/oocyte depending upon the level of expression for single-channel recording because some of the mutant AChRs were not expressed as fully as the wild type (Table 1).

Voltage Clamping. ACh-induced currents were recorded with a two-electrode voltage clamp 3–5 days after mRNA injection with the Gene Clamp 500 amplifier (Axon Instruments, Foster City, CA). Electrodes were filled with 3 M KCl and had resistances of less than 2 MΩ. Impaled oocytes in the recording chamber were perfused at a rate of 0.5 mL/s with MOR2 buffer [82 mM NaCl, 2.5 mM KCl, 5 mM MgCl$_2$, 1 mM Na$_2$HPO$_4$, 5 mM *N*-(2-hydroxyethyl)piperazine-*N*′-2-ethanesulfonic acid (HEPES), and 0.2 mM CaCl$_2$

(pH 7.4)]. ACh solutions were made from calcium-free MOR2 to avoid activation of an endogenous Ca^{2+}-dependent Cl^- current (*21*, *22*). For dose−response curve for each oocyte was held at a membrane potential of −70 mV. Membrane currents were digitized at 0.5−2 kHz and filtered at 0.1 kHz by an Axon DigiData interface (Axon Instruments) and recorded using Whole Cell Program 2.3 (kindly provided by J. Demspter) running on a Pentium III-based computer. Prisma version 3.0 (GraphPAD Software, San Diego, CA) software was utilized for data analysis and fitting. Dose−response data was collected from peak currents at nine ACh concentrations (0.1−1000 μM). The data were fit using a curve of the form $Y = 100/[1 + (EC_{50}/A)^n]$ and nonlinear regression curves. The EC_{50} and Hill coefficient values for individual oocytes were averaged to generate final estimates. Desensitization of nAChRs was assessed from the reduction in the amplitude of the peak nicotinic current induced by applied pulses of the agonist. The desensitization decays was measured by the sum of two (or more) exponentials. To describe the desensitization process, exponentials are fitted to the desensitizing and recovery phase of the current using a least-squares routine (Whole Cell Program 2.3). The general equation for the exponential fit has the following form:

$$I(t) = I_p \exp(-t/\tau) + I_{ss}$$

where $I(t)$ is the amplitude of the response at time t after the peak and I_{ss} is the steady state (nondesensitizing) current. The time constant of the relaxation is given by τ. The normalized whole-oocyte currents were analyzed by the unpaired t test from the program Instat (GraphPAD Software) to determine if the differences were statistically significant.

[^{125}I]-α-Bungarotoxin Binding Assay. The expression of nAChR in the oocyte membrane was assayed by assessing the binding of [^{125}I]-α-bungarotoxin (Amersham Life Sciences, Arlington Heights, IL) to intact oocytes according to ref *10*. From 6 to 35 oocytes per mutation were incubated in 10 nM [^{125}I]-α-bungarotoxin with 5 mg/mL bovine serum albumin in MOR2 at room temperature for 2 h, and the excess toxin was removed by washing five times with 1 mL of MOR2. To determine the normalized functional response to ACh, the [^{125}I]-α-bungarotoxin binding assay was performed immediately following voltage clamping. Noninjected oocytes were used as a background for nonspecific binding. A standard curve was obtained by counting 0−20 μL of 1 nM [^{125}I]-α-bungarotoxin solution (equivalent to 0−20 fmol). Using this approach, we can determine the normalized channel response to ACh. This is defined as the peak of the ACh-induced current (nanoamperes) per femtomole of surface α-bungarotoxin binding sites.

Patch Clamping. The oocyte vitelline membrane was removed manually after incubation in a hypertonic solution composed of 150 mM NaCl, 2 mM KCl, 3% sucrose, and 5 mM HEPES (pH 7.6). The oocytes were placed in a recording chamber containing bath solution [100 mM KCl, 1 mM $MgCl_2$, and 10 mM HEPES (pH 7.2)] at 20−22 °C. The patch pipets were made of thick-walled borosilicate glass (Sutter Instruments, Novato, CA) exhibiting resistances of 8−12 MΩ. The pipet solution contained 100 mM KCl, 10 mM HEPES, 10 mM EGTA (pH 7.2), and 4.0 or 100 μM ACh. All experiments were performed in a cell-attached

patch configuration. Single-channel currents were recorded using an AxoPatch 200B amplifier (Axon Instruments), filtered at 5 kHz (Frequency Devices Inc., Haverhill, MA), and stored on VHS tapes using a digital data recorder (VR-10B, Instrutech Corp., Mineola, NY).

Single-Channel Analysis. Data were played back into a Pentium III-based computer through a DigiData 1200 digital interface (Axon Instruments) as an analogue signal with redigitalization at 20 kHz (FETCHEX, Axon Instruments). Records were digitally filtered (Gaussian low-pass filter; net effective frequency of 4−7 kHz), and single-channel currents were detected with a half-amplitude crossing algorithm. A homogeneous set of burst is selected using LPROC (*23*). For the burst-oriented analysis, we fitted a log binwith of all the closed interval durations to the sum of three to five exponentials, and clusters of openings were defined by a critical time τ_{crit}, which was 3−5 times longer than the predominant closed time. τ_{crit} ranged from ∼300 to 10 ms at 100 μM ACh.

At all ACh concentrations, more than 70% of the close intervals belong to one exponentially distribution; τ_{crit} is set to be 3−5 times greater than the time constant of this component ($3-5t_c = b_{term}$). After b_{term} has been established, a list of bursts fulfilling this time is generated. The list is further analyzed according to the following criteria: mean amplitude, number of intervals, mean open interval duration, and probability of being open. The ranges used for each of these parameters are estimated by examining the means and the variances for the entire record. This selection procedure reduced the contribution of currents from dissimilar conductance and kinetic forms of cholinergic receptor. After a subset of bursts is selected, a list of open and close durations within those bursts is performed. The *maximum likelihood* function was used to fit the generated histogram. The PSTAT analysis software in Pclamp6 (Axon Instruments) was used to generate the fit.

RESULTS

Expression of Mutant AChRs. Twelve amino acid residues in the M4 domain of the α subunit of *T. californica* nAChR were mutated to tryptophan following injection of RNA transcribed from each mutated α subunit DNA along with wild type β, γ, and δ subunit RNAs into *X. laevis* oocytes. The level of cell-surface expression of mutant AChRs was assessed by the [^{125}I]-α-bungarotoxin ([^{125}I]BgTx) binding assay. As summarized in Table 1, the expression levels of mutants C412W, G421W, S424W, and V425W were almost the same as that of the wild type. Four mutants (L416W, I419W, I420W, and V423W) had relatively lower expression levels than the wild type, and I417W exhibited no detectable [^{125}I]BgTx binding on the surface of oocytes. These results suggest that the M4 transmembrane domain can tolerate a bulky hydrophobic side chain at all positions except αI417.

Ion Channel Properties of Mutant AChRs. To examine the ion channel function of the mutants, the ACh-induced currents were measured by two-electrode voltage clamping. ACh (300 μM) was used to measure the maximum currents for wild type and mutant AChRs since that concentration of ACh is higher than EC_{50}s for any functional AChR (as described below). The protocol for normalizing the ACh-

induced response is to apply a single ACh concentration of 300 μM per oocyte and then to normalize the amount of current measured to the toxin binding sites in the oocyte surface (nanoamperes per femtomole). This ACh concentration was selected on the basis of the dose–response curve of the wild type *Torpedo* AChR (*11*). The current for mutant I417W was not detected at holding potentials from −140 to 140 mV, whereas other mutants exhibited current amplitudes in the range of 400−2200 nA/fmol at −70 mV. These results demonstrate that mutant α subunits except I417W form functional AChRs. The maximum currents induced by ACh were normalized for the number of receptors expressed on the cell surface as shown in Table 1.

Effects of Mutations on the EC₅₀s for ACh. The EC_{50}s values for wild type and all M4 mutants are listed in Table 1. Mutations C412W, C418W, G421W, and V425W slightly decreased the EC_{50} for ACh. Other mutations (M415W, L416W, I419W, I420W, T422W, V423W, and S424W) increased the EC_{50} for ACh 3−10-fold. Except for mutant V425W ($n_H = 1.0 \pm 0.02$), there were no significant changes in the Hill coefficients of 11 tryptophan substitutions, indicating that these mutations change the EC_{50} for ACh without dramatic changes in the cooperativity of ACh binding.

Electrophysiological Results. (1) Macroscopic Current Analysis of the V425W Mutant. Previously, we found that the αC418W mutation was the most prominent mutation in the M4 domain of the *Torpedo* AChR (*10−12*). Although other mutants such as C412W and G421W exhibited a reduction in the EC_{50}, these mutations did not produce an increase in the extent of the macroscopic response to ACh (*18*). Of the present tryptophan mutants, V425W exhibited a reduction in EC_{50} and a modest increase in the extent of the normalized response to ACh. The macroscopic current and single-channel behavior of the V425W mutant were further examined. Figure 1 shows macroscopic current traces elicited by increasing ACh concentrations (1, 10, 30, 100, and 300 μM) for the wild type and V425W (A). As shown, the V425W mutant shows an increase in the extent of the macroscopic response at all ACh concentrations; however, the extent of the response of this mutation is higher at lower ACh concentrations. The normalized dose–response curves for the wild type and V425W are shown in Figure 1B. At all ACh concentrations, the V425W mutant shows a higher macroscopic response level, and the EC_{50} for V425W is 14.26 and for the wild type is 20.63. Another important observation is that the current decay time for the V425W is shorter at low ACh concentrations than that of the wild type, while at higher concentrations, it becomes similar to that of the wild type (Figure 1C).

(2) Single-Channel Data. To further examine the effects of tryptophan substitutions on channel kinetics, we examined the single-channel behavior of the wild type, C418W, and V425W. Single-channel currents were detected in cell-attached patches in *X. laevis* oocytes at −100 mV, 4.0 and 100 μM ACh, and 5 kHz, sampling for 20 μs at 22 °C. Figures 2 and 3 show single-channel traces and open time histograms recorded with oocytes expressing the wild type, C418W, and V425W at 4.0 and 100 μM ACh, respectively. Table 2 shows mean open time values for the wild type, C418W, and V425W at 4.0 and 100 μM ACh. Open time distribution for all the AChRs that were examined showed
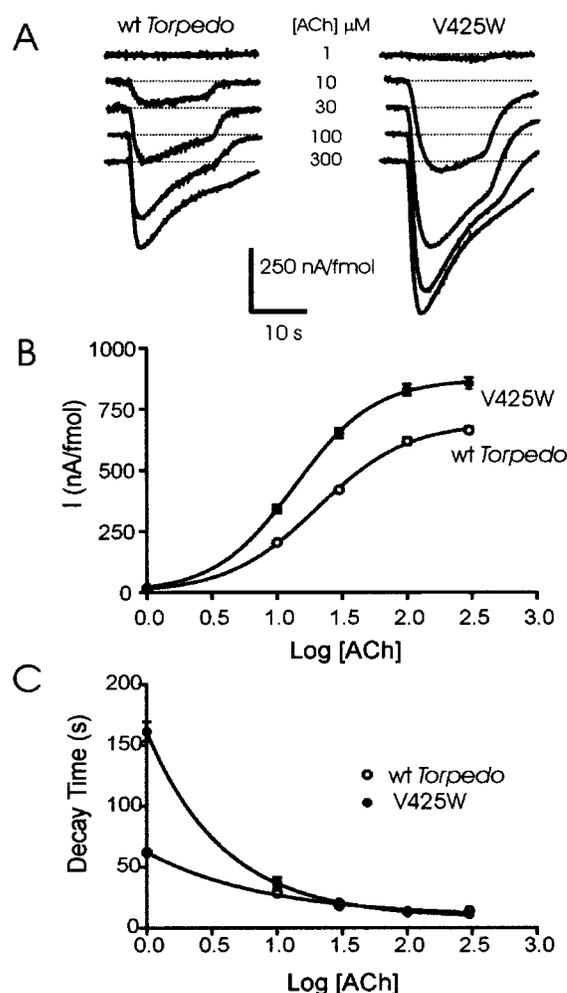

FIGURE 1: Analysis of acetylcholine-induced macroscopic responses for the wild type and V425W. Oocytes in the recording chamber were perfused at a rate of 0.5 mL/s with MOR2 buffer containing the agonist, and ACh-induced currents were detected at a membrane potential of −70 mV digitized at 2 kHz. Dose–response data were collected from peak currents at nine ACh concentrations (1.0− 300 μM). The data were fit using a curve of the form $Y = 100/[1 + (EC_{50}/A)^n]$ and nonlinear regression curves. The EC_{50} and Hill coefficient values for individual oocytes were averaged to generate final estimates. Desensitization of nAChRs was assessed from the reduction in the amplitude of the peak nicotinic current induced by applied pulses of the agonist. The desensitization decays was measured by the sum of two (or more) exponentials. (A) Macroscopic currents for the wild type and the V425W mutant at increasing ACh concentrations. (B) Normalized dose–response curves for the wild type and V425W. (C) Analysis of desensitization decay times for the wild type and V425W. At low ACh concentrations (1−10 μM), the decay time of the V425W is shorter than that of the wild type; however, at higher ACh concentrations (30− 300 μM), both decay times are very similar.

two components. At 4.0 μM ACh, the wild type exhibits open time constants of 0.069 ms ($f = 0.195$) and 0.168 ms ($f = 0.778$) and C418W 4.64 ms ($f = 0.967$) and 0.303 ms ($f = 0.033$). V425W exhibited a markedly longer open time of 23.06 ms ($f = 0.919$) with a smaller component of 0.436 ms ($f = 0.081$). At 100 μM ACh, the intraburst open time distributions for the wild type, C418W, and V425W exhibit the following values: 0.062 ms ($f = 0.514$) and 0.275 ms ($f = 0.486$), 0.277 ms ($f = 0.887$) and 2.127 ms ($f = 0.113$), and 0.64 ms ($f = 0.597$) and 2.89 ms ($f = 0.403$), respectively. At a holding potential of −100 mV, no

Table 2: Single-Channel Parameters[a]

AChR	[ACh] (μM)	no. of events (patches)	τ_{O1} (ms)	fraction	τ_{O2} (ms)	fraction	closing rate ($1/\tau_O$) α_1 (s^{-1})	α_2 (s^{-1})
wild type	4	21032 (5)	0.069	0.195	0.168	0.805	14492	5952
	100	9132 (2)	0.062	0.514	0.275	0.486	16130	3636
C418W	4	20963 (3)	0.303	0.033	4.64	0.967	3300	216
	100	34306 (3)	0.217	0.887	2.127	0.113	4608	470
V425W	4	6049 (6)	0.436	0.081	23.06	0.919	2294	43.4
	100	6375 (4)	0.064	0.597	2.891	0.403	15625	346

[a] Single-channel data were recorded in cell-attached patches at a holding potential of -100 mV, 5 kHz, and 22 °C. The sampling was set to 20 μs for data acquisition.
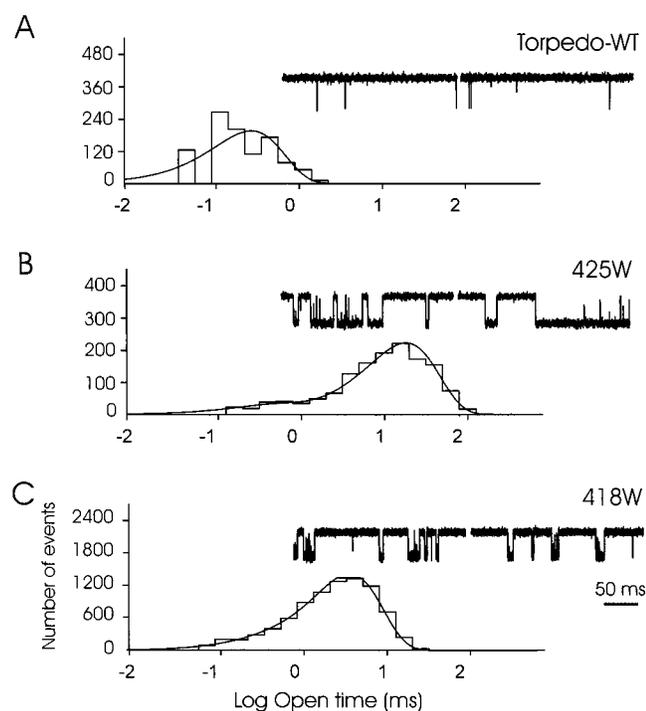

FIGURE 2: Single-channel currents for the wild type, C418W, and V425W recorded in cell-attached patches at -100 mV, 4.0 μM ACh (5 kHz, -3 db), and 22 °C. Current traces and open time histograms distributions for the wild type (A), V425W (B), and C418W (C). The open time distribution for all AChRs that were examined exhibited two components. The wild type (A) shows open time constants of 0.069 ms ($f = 0.195$) and 0.168 ms ($f = 0.778$) and C418W (C) 4.64 ms ($f = 0.967$) and 0.303 ms ($f = 0.033$). The V425W (B) showed a markedly longer open time of 23.06 ms ($f = 0.919$) with a smaller component of 0.436 ms ($f = 0.081$).

FIGURE 3: Single-channel records of bursts for the wild type, C418W, and V425W recorded in cell-attached patches at -100 mV, 100 μM ACh (5 kHz, -3 db), and 22 °C. Current traces and intraburst open time interval distributions for the wild type (A), V425 (B), and αC418W (C). The intraburst open time distributions are as follows: 0.062 ms ($f = 0.514$) and 0.275 ms ($f = 0.486$) for the wild type (A), 0.64 ms ($f = 0.597$) and 2.89 ms ($f = 0.403$) for V425W (B), and 0.277 ms ($f = 0.887$) and 2.127 ms ($f = 0.113$) for C418W (C).

significant changes in the conductance were observed in any mutant AChRs. None of the mutations altered reversal potentials.

DISCUSSION

In the study presented here, we analyzed the contribution of 12 positions of the M4 transmembrane segment of the *Torpedo* α subunit to AChR function. [^{125}I]-α-Bungarotoxin binding assays on the *X. laevis* oocytes expressing wild type and mutant AChRs demonstrated that tryptophan residues can be accommodated along the entire M4 domain of the α subunit except at position I417. The mutation of an isoleucine at position 417 in the wild type to a tryptophan residue is less drastic than many other mutations, such as glycine (at position 421) or serine (at position 424) to tryptophan. Since
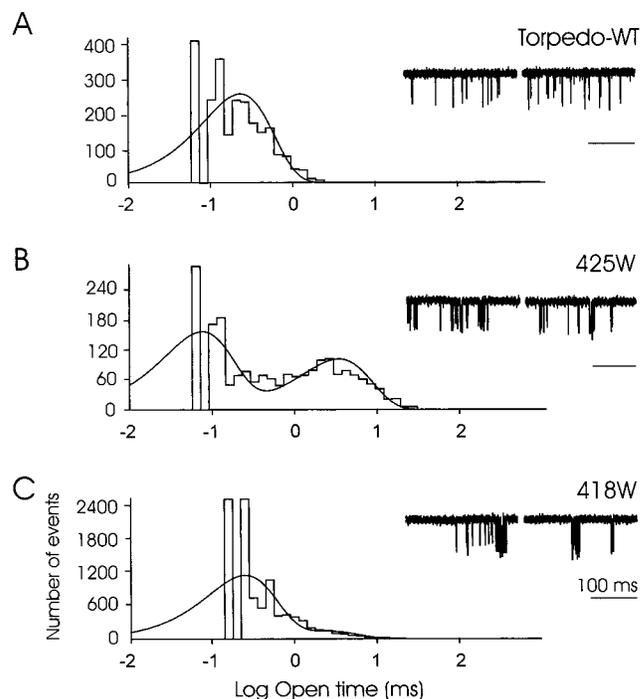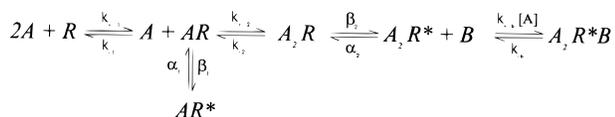
I417W is the only mutant that does not express functional receptor in this study, we speculated that this M4 position is critical for the AChR folding, oligomerization, and perhaps transport to the membrane. It is likely that the I417 might have a close contact with residues from other domains or it might be closely packed to maintain the protein structure in the membrane. Mutants L416W, I419W, I420W, and V423W showed significant reduced expression levels compared to that of the wild type. Of these four, L416W, I419W, and I420W have less than 20% of the expression levels of the wild type (Table 1). The reduced levels of expression of these three mutants suggest that the efficiency in receptor assembly or oligomerization is substantially reduced by the tryptophan substitution. Seven of the present mutations shifted the EC$_{50}$s to higher concentrations compared to wild type (Table 1). Photolabeling studies detected no labeling of the three most inhibitory mutations, L416W, I420W, and I419W, suggesting that these positions are facing the protein interior away from

the membrane lipid (*8, 9*). Four mutations displayed a reduction in their EC_{50}s compared to that of the wild type (C412W, C418W, G421W, and V425W). From these four mutations, three have been shown to be exposed to the lipid interface. Three of the mutants that displaced the dose−response curve to lower agonist concentrations (C412W, C418W, and C421W) were previously examined (*18*); therefore, we decided to focus on the V425W mutation.

The macroscopic behavior of V425W demonstrated that this lipid-exposed position plays a significant role in the channel gating mechanism (Figure 1A). At lower ACh concentrations, like 10 μM, the macroscopic response of the V425W is about 6-fold greater than the wild type response. As the ACh concentration is increased, the extent of the macroscopic response of V425W is reduced to about 1.5-fold. Two possible mechanisms might explain the reduction of the extent of the macroscopic response for the V425W mutation, a faster desensitization rate, channel block, or a combination of both. At low ACh concentrations, the slow desensitization component of the V425W mutant appears to be 3-fold slower than that of the wild type, although at low ACh concentrations the uncertainties are higher due to the small current amplitudes. However, at higher ACh concentrations, the desensitization time constant measured from current decays seems to be similar to that of the wild type (Figure 1C). This result suggests that desensitization is not causing the decrease in the extent of the macroscopic response at high agonist concentrations.

We examined the single-channel parameters of V425W, C418W, and the wild type in cell-attached patches at 4.0 and 100 μM ACh. Changes in mean open times and their respective areas can be seen in Figures 2 and 3. In our early characterization of αC418, we reported a 23-fold decrease in the closing rate constant at 16−18 °C and −80 mV (*10, 11*). To compare C418W and V425W under the same conditions, single-channel data were recorded at 22 °C and −100 mV. At 4.0 μM ACh, the open time constant of the V425W mutation is 23.06 ms. This value is 4.7-fold larger than the time constant of the C418W mutant and 43-fold larger than that of the wild type. The following sequential scheme is used to interpret channel kinetics behavior based on our data:

$$2A + R \underset{k_{-1}}{\overset{k_{+1}}{\rightleftharpoons}} A + AR \underset{k_{-2}}{\overset{k_{+2}}{\rightleftharpoons}} A_2R \underset{\alpha_2}{\overset{\beta_2}{\rightleftharpoons}} A_2R^* + B \underset{k_{-b}}{\overset{k_{+b}[A]}{\rightleftharpoons}} A_2R^*B$$

$$\alpha_1 \Big\updownarrow \beta_1$$

$$AR^*$$

where R is the receptor, A is ACh, A_2R is the biliganded species, AR^* and A_2R^* are the monoligated and biliganded open states of the receptor−ligand complex, respectively, B is the blocker molecule (in this case ACh), and A_2R^*B is the blocked state of the channel. k_{+1} and k_{+2} are the binding rate constants and k_{-1} and k_{-2} the first and second dissociation rate constants for the first and second sites, respectively. α_1 and α_2 are the fast and slow closing rate constants, respectively, and β_1 and β_2 are the fast and slow opening rates, respectively. k_{+b} is the blocking rate, and k_{-b} is the rate of opening from the blocked state. At a low acetylcholine concentration (4.0 μM, Table 2), the fast and slow closing rates for the wild type are 14 492 s^{-1} (α_1) and 5952 s^{-1} (α_2), respectively. The slow closing rates estimated from the most

abundant component are 216 s^{-1} ($f = 0.967$) for C418W and 43.4 s^{-1} ($f = 0.919$) for V425W. This decrease in the closing rate explains the relative open channel probabilities of these two mutations (Figure 2B,C). Previously, we showed that the opening rate of the C418W mutant is slightly affected (*11*); thus, here we focus on the closing rates. At a high ACh concentration (100 μM), the closing rates for the wild type are 16 130 s^{-1} (α_1) and 3636 s^{-1} (α_2). For the two tryptophan substitutions, the slow closing rates (α_2) estimated from the most abundant component in the intraburst open interval distribution at 100 μM ACh are 470 s^{-1} ($f = 0.113$) for C418W and 346 s^{-1} ($f = 0.404$) for V425W. This increase in the slow closing rate α_2 as function of agonist concentration is an indication of channel block. The fast closing rates (α_1) at high ACh concentrations estimated from the intraburst open distribution are 4608 s^{-1} ($f = 0.887$) for C418W and a faster component of 15 625 s^{-1} ($f = 0.597$) for V425W. At 4.0 μM ACh, the fast closing rate α_1 of 2294 s^{-1} for V425W is a very small component ($f = 0.081$) of the intraburst open time intervals. However, the fast opening intervals become faster (15 625 s^{-1}) and predominant ($f = 0.597$) at 100 μM ACh. This significant increase in the apparent fast opening rate α_1 of V425W is not associated with any decrease in conductance (see Figure 3B). This result clearly indicates that the increase in the apparent fast closing rate α_1 was caused by an additional component due to ACh blocking events. On the basis of the scheme shown above, this rate should be contaminated with the unblocking rate of the channel (k_{-b}). In a previous work, we also showed that the closing rate of C418W exhibits a concentration dependence on ACh that clearly indicated channel block (*11*). However, from this study, it is clear that the kinetics of channel block is faster and predominant in V425W than in C418W. This result explains the decrease in the extent of the macroscopic response of the V425W mutant at high ACh concentrations.

The normalized macroscopic response for all the present M4 mutations is shown in Table 1. The data obtained from normalized values show higher functional responses for some mutants that were shown to be expressed in very low amounts compared to the wild type. As shown in Table 1, L416W (2203 nA/fmol) and I419W (1932 nA/fmol), the two most inhibitory mutants, appear to have the highest normalized response of all the mutations. This is not due simply to the low value in the determination because some mutants with low expression levels do not produce normalized responses that are higher than that of the wild type (i.e., V423W, 809 nA/fmol). Also, mutants that have the same level of expression as the wild type show response levels lower than that of the wild type (i.e., C412W and G421W) and response levels higher than the wild type (i.e., V425W and C418W). Thus, the pattern of normalized response seems to depend on the mutant itself rather than on the variation in expression level. A tempting speculation is that normalized response is perhaps a measure of the functional fraction of surface receptors. However, to answer this question, it is necessary to fully understand the factors that control the movement of receptors between the silent and functional surface pools of nAChRs.

Structural Interpretation. The overall spatial organization of the AChR has been deduced from electron cryomicroscopy of *Torpedo* electric organ (*6*), but the detailed secondary and

tertiary structures, in particular, the transmembrane domains, remain to be established. Previous topological models suggested that the four transmembrane domains are α-helical structures. However, a 9 Å image reconstruction of frozen *Torpedo* postsynaptic membranes suggested that M2 is the only α-helical structure (*24*). A lack of similar density profiles at the AChR periphery was interpreted as a possibility of β structure for M1, M3, and M4 domains. On the other hand, chemical labeling studies using 3-(trifluorom-ethyl)-3-*m*-[^{125}I]iodophenyldiazirine ([^{125}I]TID) suggested that the M4 transmembrane domain has α-helical structure on the basis of the evidence that residues Cys412, Met415, Cys418, Thr422, and Val425 on the α subunit domain were labeled in an α-helix pattern (*9*). Molecular modeling studies suggest that M1−M4 of each subunit assemble in a complex of α-helix and β-sheet structures (*25*). Deuterium exchange studies using FTIR suggested that the M4 transmembrane segment is an α-helical structure (*26, 27*). A three-dimensional structure of a synthetic peptide corresponding to putative transmembrane segment M3 of the *Torpedo* α subunit also suggests an α-helical structure (*28*). Recently, we found that the functional assembly of the mouse AChR is more vulnerable to disruptions of α-helical secondary elements than to β-structure elements in the M4 transmem-brane segment (*12*).

The data presented here provide additional experimental evidence of a potential α-helical structure for the *Torpedo* αM4 domain. Mutants that have lower levels of expression are clustered on one side of a postulated α-helical structure. As shown in the helical wheel diagram in Figure 4A, L416, I419, and I420, which expressed less than 20% of the wild type, are clustered facing the opposite side of the C418 and V425 residues, which have been shown to be exposed to the lipid. C412, M415, and T422 are also exposed to the lipid. Thus, if the four transmembrane helices are tightly packed, inhibitory mutations such as those at L416 and I420 may face the interior of the protein. These positions may be facing M3 or M1 transmembrane segments, and this is consistent with their inhibitory activities. Recently, elegant work by Sine's group demonstrated that the cause of a congenital myasthenic syndrome was the result of the V285I mutation in the M3 of the α subunit (*29*). The increase in side chain volume at this position was shown to inhibit channel function, and this M3 position was shown previously to face the interior of the protein (*9*).

Another interesting feature of these data is the fact that the two mutations that have shown to produce the most striking effects in the channel gating have the same orienta-tion in the α-helix (Figure 4A,B), the opposite of those of three of the mutations that exhibit very low expression levels. A lack of expression of the I417W mutation suggests that at this position there is a structural constraint that is critical to receptor assembly and oligomerization. A summary of the functional changes in nAChR expression and function are shown in Figure 5. EC_{50} values (Figure 5A) and nAChR expression levels (femtomoles) (Figure 5B) were plotted as a function of M4 sequence positions 415−425. This peri-odicity plot was constructed using a cubic spline curve regression function (Prisma version 3.0, GraphPAD Soft-ware). The oscillation of the function that describes these parameters as a function of positions 415−425 indicates an approximate periodicity of 3.6 amino acids (indicated with
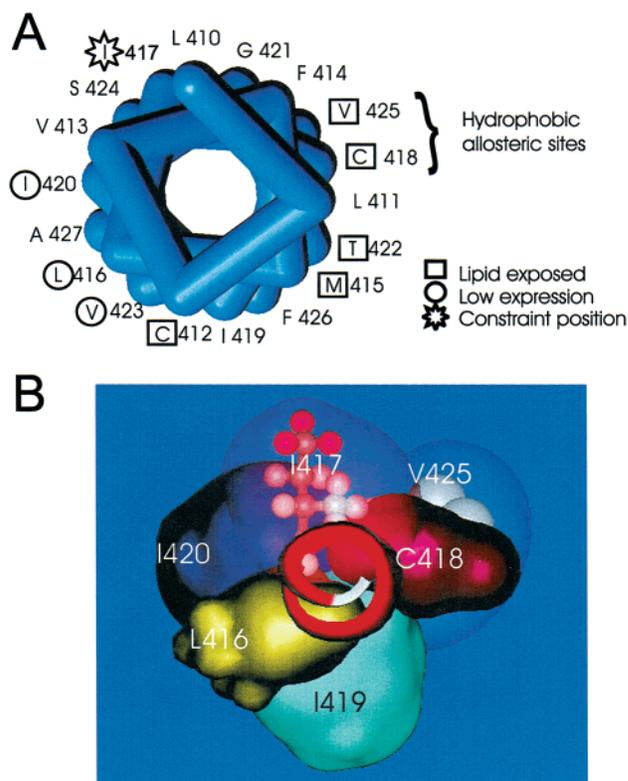

FIGURE 4: α-Helical wheel of the M4 domain of the *Torpedo* nAChR α subunit. (A) Helical view from the bottom of the α subunit M4 starting at position 410 using clockwise rotation. The diagram was constructed using 3.6 amino acids per helical turn. (B) Molecular modeling of the αM4 transmembrane segment using the same orientation. Low-expression level positions (L416, I419, and I420) and also the constraint positions (I417) are oriented to the opposite face of C418 and V425.

gray bars in Figure 5). The residues showing the highest EC_{50} values are located in the upper phase of the oscillation in Figure 5A. All of the positions in the upper phase of the oscillation, except T422, are presumably facing the interior of the protein. The same pattern is observed for the expression levels shown Figure 5B; mutants with lower expression levels are located at the lower phase of the oscillations. In summary, the overall analysis of these data together with independent data from photolabeling of *Torpedo* membranes seems to be more compatible with an α-helical structure (*8, 9*).

It is unlikely that a perturbation induced by a tryptophan substitution at positions C418 and V425 could cause a conformational alteration of the ion pore (M2) since none of the permeation (conductance) properties and ion selectivi-ties (reversal potentials) of the wild type receptor were altered by these mutations. Our structural interpretation of the results presented here seems to provide a clearer picture of how tryptophan substitutions in the M4 transmembrane domain of the nAChR alter the functional expression of the receptor as well as the channel gating mechanism. Positions that face the interior of the protein located in or near helix−helix contacts with the same or a neighboring subunit will inhibit the channel gating mechanism if the volume of the side chain is increased by a mutation. Alterations in the structure of positions that face the lipid interface are more difficult to predict. Some of the lipid-exposed positions have no
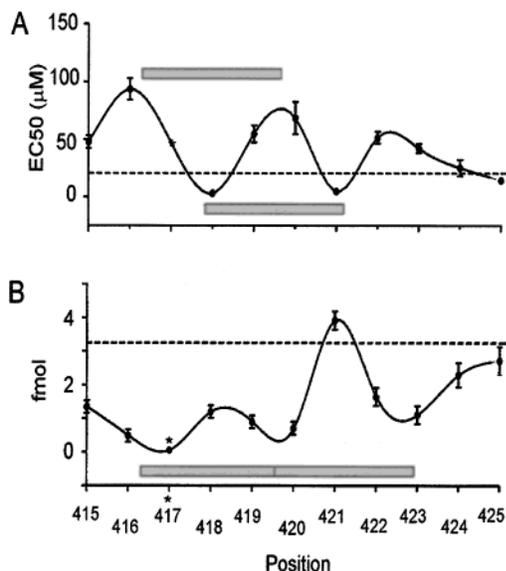
FIGURE 5: Periodicity of changes in AChR expression and function plotted as a function of tryptophan substitution at positions 415–425 in the αM4 transmembrane segment. The scale shown in the bar indicates 3.6 amino acids. The dashed line indicates the wild type value for each parameter. The asterisk indicates the I417W mutation that did not produce a functional nAChR. Plots of EC_{50} values (A) and expression levels (femtomoles) (B) vs M4 position were constructed using a cubic spline curve regression function (Prisma version 3.0, GraphPAD Software). The curves display oscillations that suggest a periodicity close to 3.6 amino acids. Each point on the *Y*-axis represents an average of a number of measurements (see Table 1).

significant effect on the channel gating mechanism if the volume of the position is increased. However, there is an exclusive group of lipid-exposed positions that are very sensitive to hydrophobic substitutions. An increase in the volume or hydrophobicity of this type of position in the AChR will increase the open probability of the channel by decreasing the closing rate via a mechanism that remains to be established.

Our experimental approach has been successful in defining functional aspects of what we propose are *hydrophobic allosteric sites* and also additional structural aspects of the AChR assembly and organization. Due to the lack of a high-resolution crystal structure, this approach has emerged as an alternative way to examine structural and functional aspects of this ligand-gated ion channel. The concept of the *hydrophobic allosteric site* represents a significant deflection from the classical notion of an "allosteric" site. Specific contacts of amino acid side chains with the lipid interface may represent another allosteric mode of interaction that remain to be defined. Finally, defining the functional role of a complex network of hydrophobic sites may lead to an understanding of the role of lipid–protein interactions in the conformational transitions of the AChR and other membrane receptor proteins.

REFERENCES

1. Arias, H. B. (1998) *Biochim. Biophys. Acta 1376*, 173–220.
2. Changeux, J. P., and Edelstein, S. J. (1998) *Neuron 21*, 959–980.
3. Karlin, A., and Akabas, M. H. (1995) *Neuron 15*, 1231–1244.
4. Galzi, J.-L., Revah, F., Bessis, A., and Changeux, J.-P. (1991) *Annu. Rev. Pharmacol. 31*, 37–42.
5. Pradier, L., and McNamee, M. G. (1992) in *The Structure of Biological Membranes*, pp 1047–1106, Telford, Caldwell, NJ.
6. Unwin, N. (1993) *J. Membr. Biol. 229*, 1101–1124.
7. Dipaola, M., Czajkowski, C., and Karlin, A. (1989) *J. Biol. Chem. 264*, 15457–15463.
8. Blanton, M. P., and Cohen, J. B. (1992) *Biochemistry 31*, 3738–3750.
9. Blanton, M. P., and Cohen, J. B. (1994) *Biochemistry 33*, 2859–2872.
10. Lee, Y.-H., Li, L., Lasalde, J., Rojas, L., McNamee, M., Ortiz-Miranda, S. I., and Pappone, P. (1994) *Biophys. J. 66*, 646–653.
11. Ortiz-Miranda, S. I., Lasalde, J. A., Pappone, P. A., and McNamee, M. G. (1997) *J. Membr. Biol. 158*, 17–30.
12. Tamamizu, S., Lee, Y.-H., Hung, B., McNamee, M. G., and Lasalde-Dominicci, J. A. (1999) *J. Membr. Biol. 170*, 157–164.
13. Fong, T. M., and McNamee, M. G. (1987) *Biochemistry 26*, 3871–3880.
14. Bhushan, A., and McNamee, M. G. (1983) *Biophys. J. 64*, 716–723.
15. Lasalde, J. A., Colom, A., Resto, E., and Zuazaga, C. (1995) *Biochim. Biophys. Acta 1235*, 427–438.
16. Barrantes, F. J. (1997) in *From Ion Channels to Cell-to-Cell Conversations* (Latorre, R., and Saenz, J. C., Eds.) pp 199–216, Plenum Press, New York.
17. Zanello, L. P., Aztiria, E., Antollini, S., and Barrantes, F. J. (1996) *Biophys. J. 70*, 2155–2164.
18. Lasalde, A. J., Tamamizu, S., Butler, D. H., Vibat, C. R. T., Hung, B., and McNamee, M. G. (1996) *Biochemistry 35*, 14139–14148.
19. Horton, R. M., and Pease, L. R. (1991) in *Directed mutagenesis* (McPherson, M. J., Ed.) pp 217–246, IRL Press, New York.
20. Pradier, L., Ye, A. S., and McNamee, M. G. (1989) *Biochemistry 28*, 6562–6571.
21. Barish, M. E. (1983) *J. Physiol. (London) 342*, 309–325.
22. Mishina, M., Kurosaki, T., Tobimatsu, T., Morimoto, Y., Noda, M., Yamamoto, T., Terao, M., Lindstrom, J., Takahashi, T., Kuno, M., and Numa, S. (1984) *Nature 307*, 604–608.
23. Neil, J., Xiang, Z., and Auerbach, A. (1991) *Methods Neurosci. 4*, 474–490.
24. Unwin, N. (1995) *Nature 373*, 37–43.
25. Ortells, M., and Lunt, G. A. (1996) *Protein Eng. 9*, 51–59.
26. Baenzinger, J. E., and Méthot, N. (1995) *J. Biol. Chem. 270* (49), 29129–29137.
27. Méthot, N., and Baenzinger, J. E. (1998) *Biochemistry 37* (42), 14815–14822.
28. Lugovskoy, A. A., Maslennikov, I. V., Utkin, Y. N., Tsetlin, V. I., Cohen, J. B., and Arseniev, A. S. (1998) *Eur. J. Biochem. 255*, 455–461.
29. Wang, H. L., Milone, M., Ohno, K., Shen, X., Tsujino, A., Batocchi, A. P., Tonali, P., Brengman, J., Engel, A. G., and Sine, S. M. (1999) *Nat. Neurosci. 2*, 226–233.